RSC Advances

ROYAL SOCIETY OF CHEMISTRY

www.rsc.org/advances

Ultra-strong gel-spun ultra-high molecular weight polyethylene fibers filled with chitin nanocrystals

Minfang An[1], Haojun Xu[1], You Lv[1], Tianchen Duan[1], Feng Tian[2], Liang Hong[3], Qun Gu[4], Zongbao Wang[1,*]

[1]Ningbo Key Laboratory of Specialty Polymers, Faculty of Materials Science and Chemical Engineering, Ningbo University, Ningbo 315211, PR China

[2]Shanghai Institute of Applied Physics, Chinese Academy of Sciences, Shanghai 201204, China

[3]Ningbo Institute of Material Technology and Engineering, Chinese Academy of Sciences, Ningbo 315201, PR China

[4]College of Material Engineering, Ningbo University of Technology, Ningbo 3151006, P. R. China

[*]Corresponding author. E-mail address: wangzongbao@nbu.edu.cn

Abstract

Ultra-high molecular weight polyethylene (UHMWPE)/chitin nanocrystals (CNC) and UHMWPE/acetylated chitin nanocrystals (ACNC) fibers were prepared. The addition of CNC and ACNC significantly enhanced the ultimate tensile strength and Young's modulus of the UHMWPE fibers matrix. Compared with that of pure UHMWPE fibers, the ultimate tensile strength and Young's modulus of UHMWPE/CNC fibers are increased about 14.5 % and 17.0 %, respectively, with the incorporation of 1.0 wt% CNC. Furthermore, with the addition of 1.0 wt% ACNC, the ultimate tensile strength and Young's modulus of UHMWPE/ACNC fibers are improved by 15.8 % and 21.3 %, respectively. To understand the mechanism of CNC

and ACNC reinforcing UHMWPE fibers, the thermal, crystallinity, orientation and shish structure of pure UHMWPE fibers, UHMWPE/CNC fibers, and UHMWPE/ACNC fibers were determined by employing differential scanning calorimeter (DSC), thermogravimetric Analysis (TGA), scanning electron microscopy (SEM), wide-angle X-ray diffraction (WAXD), and small-angle X-ray scattering (SAXS) analyses.

Keywords: UHMWPE fibers, chitin nanocrystals, acetylation, orientation, shish structure.

1. Introduction

UHMWPE fibers are high-performance fibers, which have widely been used as bullet-proof materials, high-strength ropes, and in other areas. UHMWPE fibers have high-performance due to the high orientation and crystalline of the molecular structure. The theoretical tensile strength and modulus of UHMWPE fibers are 19-26 GPa and 250-350 GPa[1], respectively, while the current reports are far from the limit value. The key point of obtaining higher performance UHMWPE fibers is to make fibers with a higher draw ratio during spinning process, and consequently more molecules can be involved in the formation of extended chain crystals. More extended chain crystals content in UHMWPE fibers makes higher degree of orientation and crystallinity, and hence better performance. Therefore, to enhance the molecular orientation and crystallization by perfecting the spinning process has become a major approach to improve the performance of UHMWPE fibers[2-10],

specially at the early stage of a fiber preparation. However, it is very limited to further improve the properties of UHMWPE fibers just simply relying on improving the spinning process.

With the rise of nanocomposite technology and its application in the field of polymer materials, the preparation of UHMWPE/nanofiller composite fibers provided a new opportunity to improve the properties of UHMWPE fibers. It was rapidly become a hot research topic to make use of nanofillers such as spherical SiO_2, layered montmorillonite (MMT) and fibrous carbon nanotube (CNT) to modify the UHMWPE fibers. Zhang et al. [11] reported that a simple treatment approach was performed to achieve the improved surface properties of UHMWPE fibers by incorporation of nano-SiO_2. The nano-SiO_2 was first dispersed in xylene in the presence of silane coupling agent to prepare the extracting solution. Then UHMWPE gel fibers were treated with the extraction solution and subsequently ultradrawn to produce UHMWPE/SiO_2 nanocomposite fibers with different compositions of nano-SiO_2. When the nano-SiO_2 content was 0.5 wt%, the mechanical properties of UHMWPE/SiO_2 fibers reached the maximum values. The tensile strength and modulus of UHMWPE/SiO_2 (0.50 %) fibers were higher than those of pure UHMWPE fibers by 23.2 % and 76.1 %, respectively. And the elongation-to-break ratio was 3.09 %, which was 0.98 % higher than that pure UHMWPE fibers. But the degree of orientation of UHMWPE/SiO_2 fibers was lower than that of pure UHMWPE fibers. Yeh et al.[12] added nanosilica into UHMWPE gel solutions to prepare UHMWPE/nanosilica composite fibers by gel-spinning, resulted in higher tensile strength, modulus and

elongation but lower melting temperature (T_m). The heat resistance of UHMWPE/nanosilica composite fibers became worse. In addition, Yeh et al.[13] obtained UHMWPE/attapulgite (ATP) composite fibers with the same method and found that the mechanical properties were significantly improved by adding 0.025 wt% ATP, the strength and modulus increased by 81.8 % and 84.7 %, respectively, but the melting temperature decreased. Ruan et al. [14] reported that the tensile strength and elongation of gel-spun UHMWPE composite fiber filled with 5 wt% multiwalled carbon nanotubes (MWCNTs) reached 4.2 GPa and 5 %, respectively, which were 18.8 % and 15.4 % higher respectively than those of pure UHMWPE fiber with the same draw ratios. But the distribution of MWCNT in UHMWPE fibers matrix was very uneven. Yeh et al. [15-19] also found that the UHMWPE nanocomposite fibers with the increased tensile strength but with relative low melting point and thinner lamellar structure were produced by adding pristine and functionalized MWCNTs, unmodified and modified bacterial cellulose (BC) nanofibers, respectively, in UHMWPE gel solutions. In one words, nanosilica, ATP, BC nanofibers, modified BC nanofibers, MWCNTs, as well as modified MWCNTs can be used to reinforce UHMWPE fibers, and ultimately improved the tensile strength of the composite fibers but lower the melting temperature. In addition, MWCNTs were difficult to be dispersed in UHMWPE fibers, although the toughness of composite fibers was improved. And the poor dispersion of MWCNTs in UHMWPE may limit the molecular chain's orientation during the hot drawing process, and as a result, may affect the further improvement of fiber performance.

From the published research results of UHMWPE/nanofiller composite fibers, CNT could be the best one to improve the toughness of UHMWPE fibers, however, the benefits were quite depended on the different materials and the processing conditions. The strength and modulus of CNT were much higher than those of pure UHMWPE fibers, therefore, it is very difficult to determine the mechanism of reinforcing UHMWPE fibers with CNTs.

Biological nanocrystals have the dimension like CNTs, which may imply that they could affect the orientation and the crystallization of fibers if they were used to modify UHMWPE fibers, e.g., to induce the formation of shish-kebab structure. Furthermore, the mechanical properties of biological nanocrystals are similar to that of pure UHMWPE fibers and much lower than that of CNTs (the tensile strength and modulus are up to 150 GPa and 1 TPa, respectively)[20], thus biological nanocrystals will affect the mechanical properties of UHMWPE fibers mainly by altering the molecular orientation and crystallization. On the surface properties, nanocrystals show strong polarity due to hydroxyl groups and amide groups rich on the surface. After chemical modification, the surface showed nonpolar[21-22], and the thermal degradation temperature was significantly improved, which created the conditions for the study of the effect of the nanofiller surface properties on the structure of UHMWPE fibers. In addition, biological nanocrystals are natural renewable resources with a wide range of sources, they not only have the nature of natural polymer such as renewable, biodegradable, non-toxic and biocompatible, but also have the characteristic of high specific surface area and high mechanical strength (the

longitudinal and transverse modulus are 150 and 15 GPa[23], respectively) as other nano-scale materials, which makes biological nanocrystals suitable to be used as organic nanofillers for a composite material system[24-25]. As early as in 1999, Dufresne et al.[26] found that nanocrystals could induce crystalline polymer to produce the transcrystalline layer structure, which played an important role in the mechanical properties of composite materials. Over the past twenty years, biological nanocrystals or modified biological nanocrystals have been used to reinforce polymer such as PLA[27], PCL[28], PHBV[21-22], PLGA[29], polyacrylamide[30] and poly (vinyl alcohol)[31]. Thus, the UHMWPE/nanocrystals composite fibers are expected to expand the application areas of UHMWPE materials.

In this study, original and acetylated chitin nanocrystals were added in UHMWPE gel solution to prepare UHMWPE/chitin nanocrystals (CNC) and UHMWPE/acetylated chitin nanocrystals (ACNC) fibers with higher mechanical properties. To investigate the actual effect of CNC and ACNC on UHMWPE fibers, our UHMWPE fibers were produced at the industrial production line. We would research the reinforced and toughened effect from the nanocrystals contents and analysis the mechanism from the structure.

2. Experimental

2.1 Materials

The UHMWPE resin used in this study is associated with a viscosity-average molecular weight ($\bar{M}_V$) of 2.7×10^6, which was supplied by Sinopec Beijing Yanshan Company. Chitin from shrimp shells was purchased from Aladdin reagent Co., Ltd.

(Shanghai, China). Chitin nanocrystals were prepared through acid hydrolysis as described in previous report[32]. Chitin whisker suspensions were prepared first by hydrolyzing the purified chitin sample in an aqueous HCl solution (3 mol/L) under stirring at boiling temperature for 1.5 h. After acid-hydrolysis, the suspensions were diluted with distilled water followed by centrifugation. This process was repeated three times. Then, the suspensions were transferred to a dialysis bag and dialyzed for 24 h against distilled water until the pH value of the suspension was 6. The residual aggregates were subsequently removed by a filtration and the suspension was kept in a refrigerator until used. Sodium azide was added to the suspension to prevent the growth of microorganisms. Finally, the chitin nanocrystals were obtained after vacuum-drying. Hydrochloric acid, potassium hydroxide, succinic acid, ptoluenesulfonic acid, dimethyl sulfoxide, glacial acetic acid, acetic anhydride, methanesulphonic acid and absolute ethyl alcohol were purchased from Sinopharm Chemical Reagent Co., Ltd. (Shanghai, China). All reagents were used as received without further purification.

2.2 Preparation of acetylated chitin nanocrystals (ACNC)

CNC were used after vacuum-drying them for 12 h. 0.5 g of the CNC and 30 ml of glacial acetic acid were placed in a 250 mL three-neck flask. Subsequently, the resultant suspension was treated under ultrasonic conditions for 10 min. After the ultra-sonication, 60 mL of acetic anhydride was added to the mixture followed by stirring for 5 min. 0.1 g of methanesulphonic acid was added to the reactor and the reaction mixture was stirred for 60 min at 45 ◦C. After modification, the suspension was centrifuged and the precipitation was washed with absolute ethyl alcohol for three times. Then the precipitation was dispersed into absolute ethyl alcohol for producing acetylated chitin nanocrystals suspension. The ACNC suspension dialyzed

using several changes of absolute ethyl alcohol.

2.3 Fabrication of UHMWPE/CNC fibers and UHMWPE/ACNC fibers

Varying contents of CNC and ACNC of 0, 0.5 and 1 wt% together with UHMWPE resin were dispersed and dissolved in paraffin oil to prepare 5 wt% UHMWPE solutions at 150 ◦C for 1 h. The UHMWPE, UHMWPE/CNC, UHMWPE/ACNC gel solutions prepared above were then fed into a temperature-controlled hopper and kept as hot homogenized gel solutions before spinning. The hot homogenized gel solutions were then gel-spun using spinneret plate with 240 conical dies with an exit diameter of 1 mm at an extrusion rate of 2000 mm/min and an extrusion temperature of 248 ◦C. The gel-spun fibers were then extracted in a dichloromethane bath to remove the residual paraffin oil. Finally, fibers were gone through three hot drawing stages with 49 draw ratios. To investigate the actual effect of CNC and ACNC on UHMWPE fibers, our UHMWPE fibers production process was completely replicating the industrial production line.

2.4 Thermal analysis

Differential scanning calorimetry (DSC) measurements were performed with a Mettler Toledo DSC under nitrogen atmosphere. The samples of fibers were prepared by cutting into pieces. The samples of pure UHMWPE fibers, UHMWPE/CNC fibers and UHMWPE/ACNC fibers were heated to 180 ◦C at a heating rate of 10 ◦C/min under flowing nitrogen at a flow rate of 50 mL/min. Samples weighing 6.0 mg were

placed in the standard aluminum sample pans for determination of their melting temperature (T_m). Thermogravimetric analysis (TGA) was performed on a TG/DTA 7300 apparatus. The samples were heated at a rate of 10 °C/min under a flow of nitrogen (50 mL/min) from 25 to 550 °C.

2.5 Tensile test

Tensile test of pure UHMWPE fibers, UHMWPE/CNC fibers and UHMWPE/ACNC fibers with no twisting was performed on an Instron 5567 tension testing machine at a tensile rate of 250 mm/min, and the fiber initial gauge length was 500 mm.

2.6 The SAXS and WAXD measurement

The wide-angle X-ray diffraction (WAXD) and small-angle X-ray scattering (SAXS) measurements were carried out at the BL16B1 beamline in the Shanghai Synchrotron Radiation Facility (SSRF). The wavelength of the synchrotron radiation was 0.124 nm. Two-dimensional (2D) WAXD and SAXS patterns were collected by using a Mar CCD X-ray detector (MAR165), having a resolution of 2048×2048 pixels. The beam intensity monitor before sample was a N_2 gas ionization chamber, and the monitor after sample adsorption was a photodiode in the beam stop. Two scatter-less slits (Xenocs) were used to depress parasitic scattering. The sample holder was mounted onto an optical table[33]. The sample-to-detector distance was 5080 mm for SAXS and 213 mm for WAXD. The SAXS and WAXD image acquisition time of each data frame was 20 s and 2 s, respectively. All X-ray images were corrected for background

scattering, air scattering, and beam fluctuations. The WAXD and SAXS measurement date analysis were carried out by the Fit2d software package [34].

2.7 SEM

The surface morphologies of pure UHMWPE fibers at different drawing stages were observed by scanning electron microscopy (SEM) (SU8010). The samples were sputtered with gold before SEM observation.

3. Results and discussion

3.1 Tensile test

Samples identification and CNC and ACNC content in the UHMWPE composite fibers are shown in Table 1. Fig.1 shows the stress–strain curves of pure UHMWPE fibers, UHMWPE/CNC fibers, and UHMWPE/ACNC fibers. Tests were performed on ten different specimens at least for each composition, and the average tensile values with the standard deviation are summarized in Table 2. The addition of CNC and ACNC significantly enhanced the ultimate tensile strength and Young's modulus of UHMWPE fibers. It may be because that CNC and ACNC play an important role in inducing the formation of shish-kebab structure[26]. Compared with pure UHMWPE fibers, the ultimate tensile strength and Young's modulus of UHMWPE/CNC fibers are improved by about 14.5 % and 17.0 %, respectively, with the incorporation of 1.0 wt% CNC. Moreover, with the addition of 1.0 wt% ACNC, the ultimate tensile strength and Young's modulus of UHMWPE/ACNC fibers are improved by 15.8 % and 21.3 %,

respectively. These results indicate that ACNC have more effective influence on the mechanical properties of UHMWPE fibers than the original CNC. The reason may be that ACNC has better dispersion than the original CNC in the UHMWPE fibers matrix. In previous work[22], we dispersed the CNC and ACNC in ethyl alcohol solution, respectively, with ultra-sonication and observed with transmission electron microscopy (TEM). After sonication, there was still a small amount of CNC aggregation in the suspension, while aggregation of ACNC was not observed. In conclusion, the aggregation degree of ACNC has been reduced after modification. In this study, CNC and ACNC were dispersed in paraffin oil. Comparable results in regards to a small amount of aggregation of CNC and no aggregation of ACNC were confirmed. It was very easy to form hydrogen bonds between CNC due to the surface hydroxyl groups. After acetylation ACNC retained a rod-like morphology and crystal structure compared with original CNC, and that the hydroxyl groups were partly replaced by acetyl groups on surface of CNC. Moreover, the hydrophobicity of CNC was counteracted by introduction of hydroxyl groups.

3.2 Thermal analysis

Typical differential scanning calorimeter (DSC) thermosgrams of pure UHMWPE fibers, UHMWPE/CNC fibers and UHMWPE/ACNC fibers are shown in Fig.2 and the melting temperature (T_m) are shown in Table 3. The melting temperature (T_m) of pure UHMWPE fibers, UHMWPE/CNC fibers and UHMWPE/ACNC fibers almost has no difference. But the bottom of main melting peak of UHMWPE composite fibers with

0.5 and 1.0 wt% CNC is sharper than others. The DSC thermograms of all fibers have a small peak at about 159 ◦C. The endotherm peak (159 ◦C) is from melting of the hexagonal crystalline structure and possibly from randomization of chains to the gauche state in the melt.[35] In DSC thermograms, the peaks (159 ◦C) of UHMWPE/CNC fibers were weaker than pure UHMWPE fibers and UHMWPE/ACNC fibers. The reason may be that the process from randomization of chains to the gauche state in the melt was hindered by the agglomeration of CNC. This might also be responsible for the base onset of the main melting peak of UHMWPE/CNC fibers being sharper than those relating to other fibers and composites.

Fig. 3 shows the TGA curves of pure UHMWPE fibers, UHMWPE/CNC fibers, and UHMWPE/ACNC fibers. The decomposition temperature at 5 % weight loss ($T_{d,\ 5\%}$) and at the maximum rate ($T_{d,\ max}$) are listed in Table 3. The addition of CNC and ACNC improved the thermal stability of UHMWPE fibers matrix, while UHMWPE/ACNC fibers exhibits higher thermostability than that of UHMWPE/CNC fibers. Different to that of UHMW PE/inorganic composite fibers, both of UHMWPE/CNC and UHMWPE/ACNC composite fibers had almost no residual confirmed by TGA measurements, when the temperature increased to above 520 ◦C (Fig. 3). This result could be easily understood because the onset decomposition temperature of CNC (277.8 ◦C[36]) is close to that of UHMWPE fibers. Therefore, the little effect of ACNC on the thermostability of UHMWPE fibers could be due to the structural variation of UHMWPE fibers.

3.3 Crystallinity Change

2D WAXD patterns (Fig.4) were analyzed to calculate the degree of crystallinity of pure UHMWPE fibers and UHMWPE/CNC fibers from eq 1.

$$X_c = \frac{I_c}{I_t} \quad I_t = I_c + I_a \qquad (1)$$

where I_c and I_a represent the integrated diffraction intensity of the crystal phase (sum of $(010)_m$, $(110)_o$ and $(200)_o$ reflections) (Fig.6) and the scattered intensity of the amorphous phase, respectively. It is the integrated diffraction intensity (azimuthal angle,$\emptyset = 0 - 360°$) due to the sum of amorphous and crystal phases. The WAXD profile was curve-fitted by applying Voight functions.

Fig.5 shows the SEM images of different stages of pure UHMWPE fibers. The shish-kebab structure could be observed obviously in Fig.5 (b), however, the kebab structure could not be observed in the SEM images of finished fibers (Fig.5 (c, d)). Numerous pioneer works[3-10] reported that the shish-kebab structure was commonly found as the morphology of drawn fibers of early hot-drawing stage in the fabrication process of UHMWPE fibers. With the increase of hot-drawing ratio, the kebab crystal converted gradually to the extended chain crystal, in other words, most of kebab structure converted to shish structure eventually. So the kebab structure disappeared in the SEM images of produced fibers with high drawing ratio as Fig.5 (c, d). The 2D SAXS images of various UHMWPE fibers are shown in Fig.4. The scattering patterns of shish structure could be observed instead of kebab scattering patterns, which were in match with SEM observation (Fig.5 (c, d)).

Fig.6 shows the 1D WAXD intensity profiles of pure UHMWPE fibers, UHMWPE/CNC fibers and UHMWPE/ACNC fibers. Comparing from the intensity and

position of diffraction peaks $(010)_m$, $(110)_o$, $(200)_o$, there is no any obvious difference between various fibers intensity profiles. The degree of crystallinity of pure UHMWPE fibers, UHMWPE/CNC fibers and UHMWPE/ACNC fibers is shown in Table 4. The addition of CNC and ACNC significantly enhanced the degree of crystallinity of the UHMWPE fibers matrix. Compared with pure UHMWPE fibers, the degree of crystallinity of UHMWPE/CNC0.5 fibers and UHMWPE/ACNC0.5 fibers are improved by about 1.4 % and 2.6 %, respectively, while the degree of crystallinity of UHMWPE/CNC1.0 fibers and UHMWPE/ACNC1.0 fibers are improved by about 7.2 % and 16.9 %, respectively. The reason might be that both CNC and ACNC could induce the shish-kebab structure formation and ACNC have better dispersion than the original CNC in the UHMWPE fibers matrix. And it makes that ACNC could be better to provide nucleation sites for UHMWPE molecular chains so that much more molecules took part in crystallization, comparing with CNC. So the degree of crystallinity of UHMWPE/ACNC fibers is significantly higher than UHMWPE/CNC fibers. In addition, the size of CNC is 20-40 nm wide and 150-400 nm long (The related characterization of CNC and ACNC was presented detailedly in our previous paper)[22], which are very similar to the size of shish in UHMWPE fibers. So CNC and ACNC might act as the shish of UHMWPE fibers that formed in the early stage, which provides nucleation sites for the formation of kebab. Therefore much more molecules took part in the formation of shish-kebab structure and then involved in the formation of extended chain crystal.

3.4 Crystalline orientation

Quantitatively, the degree of crystal orientation in pure UHMWPE fibers, UHMWPE/CNC fibers and UHMWPE/ACNC fibers was determined by using the Herman's method[37]. Accordingly, the crystalline orientation can be characterized by average orientation of the normal to the crystalline plane with respect to an external reference frame. Here, the flow direction was taken as the reference direction. For a set of hkl planes, the average orientation, expressed as $\langle\cos^2\emptyset\rangle_{hkl}$, can be calculated mathematically using the following equation:

$$\langle\cos^2\emptyset\rangle_{hkl} = \frac{\int_0^{\pi/2} I(\emptyset)\cos^2\emptyset \sin\emptyset d\emptyset}{\int_0^{\pi/2} I(\emptyset)\sin\emptyset d\emptyset} \qquad (2)$$

where $\emptyset$ is the azimuthal angle and $I(\emptyset)$ is the scattered intensity along the angle $\emptyset$. Herman's orientation function, f, is defined as

$$f = \frac{3\langle\cos^2\emptyset\rangle_{hkl} - 1}{2} \qquad (3)$$

where f has the value of -0.5, when the normal of the reflection plane is perpendicular to the reference direction ($\emptyset = 90°$ or crystals are oriented parallel to the fiber axial direction), a value of 1, when the normal is parallel to the reference direction ($\emptyset = 0°$ or crystals are oriented perpendicularly to the fiber axial direction), and a value of 0, when the orientation is random. The degree of orientation, f_{110} and f_{200}, are calculated from the azimuthal intensity distribution, $I(\emptyset)$, of the (110)

reflection and the (200) reflection, respectively, of a-crystals in pure UHMWPE fibers, UHMWPE/CNC fibers and UHMWPE/ACNC fibers.

Table 4 shows the degree of orientation, f_{110} and f_{200}, of pure UHMWPE fibers, UHMWPE/CNC fibers and UHMWPE/ACNC fibers. Compared with pure UHMWPE fibers, the degree of orientation of UHMWPE/CNC fibers and UHMWPE/ACNC fibers are both slightly reduced. But the degree of orientation is almost no difference between of UHMWPE/CNC fibers and UHMWPE/ACNC fibers with varying content of CNC and ACNC. The result indicates that CNC and ACNC are not conducive to improve the degree of orientation of UHMWPE fibers matrix. The reason could be that only partial axial direction of CNC and ACNC was well parallel to the fiber axial direction during the process.

3.5 Shish structure

To better investigate the role of CNC and ACNC on the formation of shish structure in UHMWPE fibers matrix, the changes of the average shish length, $\langle L_{shish} \rangle$, and the misorientation of shish, $B_{\emptyset}$, were followed. These parameters were obtained by using the Ruland streak method to analyze the equatorial streak feature in SAXS.[38-40] Ruland demonstrated that the size and orientation distributions of longitudinal voids in polymer and carbon fibers in real space could be estimated from the equatorial streak of SAXS in reciprocal space (as long as the orientation and the longitudinal length of scatterer are finite). Since the method is principally based on the separation of experimentally measured azimuthal breadth from contributions of scatterer length

and misorientation, the method can also be applied to separate the average length of shish and its average misorientation. If one assumes that all azimuthal distributions can be modeled by Lorentz functions, the observed azimuthal width, Bobs, can be related to the length of shish, $\langle L_{shish} \rangle$, and the azimuthal width, $B_{\emptyset}$, due to misorientation of shish by the following equation.

$$B_{obs} = \frac{1}{\langle L_{shish} \rangle s} + B_{\emptyset} \quad (4)$$

If all azimuthal distributions have Gaussian expressions, then the relationship becomes

$$B_{obs}{}^2 = \left(\frac{1}{\langle L_{shish} \rangle s}\right)^2 + B_{\emptyset}{}^2 \quad (5)$$

where B_{obs} represents the integral width of the azimuthal profile from the equatorial streak at s. On the basis of eq 4 or eq 5, $\langle L_{shish} \rangle$ can be obtained from the slope, and the misorientation width, $B_{\emptyset}$ can be obtained from the intercept of the plots (B_{obs} vs s^{-1} or B_{obs}^2 vs s^{-2}). In this study, we found that all azimuthal distributions were better fit with Lorentz functions, thus the plot based on eq 4 (as shown in Fig. 7.) was used to determine $\langle L_{shish} \rangle$ and $B_{\emptyset}$.

Fig.4 shows the 2D WAXD and SAXS images of various UHMWPE fibers. It is difficult to find the difference between pure UHMWPE fibers, UHMWPE/CNC fibers and UHMWPE/ACNC fibers in 2D SAXS images. The average shish length ($\langle L_{shish} \rangle$)

and the shish misorientation ($B_{\emptyset}$) of pure UHMWPE fibers, UHMWPE/CNC fibers and UHMWPE/ACNC fibers are shown in Table 5. The average shish length ($\langle L_{shish} \rangle$) and the shish misorientation ($B_{\emptyset}$) of UHMWPE/ACNC fibers are both improved with the addition of the content of ACNC. But with the addition of the content of CNC, the average shish length ($\langle L_{shish} \rangle$) and the shish misorientation ($B_{\emptyset}$) of UHMWPE/CNC fibers are both decreased. The result indicates that the longer shish is easy to form in UHMWPE/ACNC fibers, which plays an important role in enhancing the properties of UHMWPE fibers. It may be because that ACNC is beneficial to the transformation from kebabs to shishs in UHMWPE fibers.[7] But the shish in UHMWPE/CNC fibers was easier to break. The reason may be that the agglomeration of CNC was relatively obvious in UHMWPE fibers matrix, while ACNC was easy to disperse. And the agglomeration of CNC has hindered the transformation from kebab to shish in UHMWPE/CNC fibers.

4. Conclusions

The addition of CNC and ACNC significantly enhance the ultimate tensile strength and Young's modulus of the UHMWPE fibers matrix with almost no effect on the melting temperature (T_m). The thermal stability of UHMWPE fibers matrix has been improved with the addition of CNC and ACNC, while the thermal stability of UHMWPE/ACNC fibers is better than that of UHMWPE/CNC fibers. Compared with pure UHMWPE fibers, the crystallinity of UHMWPE/CNC fibers and UHMWPE/ACNC fibers are both improved. And the mechanical properties and crystallinity of

UHMWPE/ACNC fibers are better than UHMWPE/CNC fibers with the same content of nanofillers. In addition, the degree of orientation of UHMWPE/CNC fibers and UHMWPE/ACNC fibers are both slightly reduced. But the degree of orientation is almost no difference between of UHMWPE/CNC fibers and UHMWPE/ACNC fibers with varying content of CNC and ACNC. In the shish structure, ACNC is conducive to the formation of long shish in UHMWPE fibers matrix, while CNC leads to the break of shish. The above results suggest that the excellent properties of the UHMWPE nanocomposite fibers can be obtained by UHMWPE fibers with the optimal contents and well dispersed ACNC. To better understanding the structural effect of chitin on UHMWPE fibers matrix, the investigation of in-situ structural evolution of UHMWPE/CNC fibers is ongoing.

Acknowledgements

This work was supported by the National Science Foundation of China (51273210 and 51003117), Open Research Fund of State Key Laboratory of Polymer Physics and Chemistry, Changchun Institute of Applied Chemistry, Chinese Academy of Sciences and K. C. Wong Magna Fund in Ningbo University. We thank Shanghai Synchrotron Radiation Facility (SSRF) for supporting the WAXD and SAXS tests.

References

1. J. Smook, W. Hamersma and A. J. Pennings, *Journal of materials science,* 1984, **19**, 1359-1373.

2. A. J. Pennings and J. Smook, *Journal of Materials Science,* 1984, **19**, 3443-3450.

3. W. Hoogsteen, R. J. van der Hooft, A. R. Postema, G. ten Brink and A. J. Pennings, *Journal of materials science,* 1988, **23,** 3459-3466.

4. J. P. Penning, A. A. D. Vries and A. J. Pennings, *Polymer Bulletin,* 1993, **31,** 243-248.

5. B. Kalb and A. J. Pennings, *Polymer*, 1980, **21,** 3-4.

6. T. Kanamoto, A. Tsuruta, K. Tanaka and M. Takeda, *Macromolecules,* 1988, **21**, 470-477.

7. Y. Ohta, H. Murase and T. Hashimoto, *Journal of Polymer Science Part B: Polyme Physics,* 2010, **48**, 1861-1872.

8. J. T. Yeh, S. C. Lin, C. W. Tu, K. H. Hsie and F. C. Chang, *Journal of materials science,* 2008, **43**, 4892-4900.

9. T. Jian, W. D. Shyu, Y. T. Lin, K. N. Chen and J. T. Yeh, *Polymer Engineering and Science,* 2003, **43**, 1765-1777.

10. Y. Ohta, H. Murase and T. Hashimoto, *Journal of Polymer Science Part B: Polymer Physics,* 2005, **43**, 2639-2652.

11. Y. Zhang and J. R. Yu, C. G. Zhou, L. Chen and Z. M. Hu, *Polymer Composites,* 2010, **10**, 684-690.

12. J. T. Yeh, C. K. Wang, A. Yeh, L. K. Huang, W. H. Wang, K. H. Hsieh, C. Y. Huang and K. N. Chen, *Polymer International,* 2013, **62**, 591-600.

13. J. T. Yeh, C. K. Wang, C. C. Tsai, C. H. Lin, C. Y. Huang, K. N. Chen, K. S. Huang and S. H. Chiu, *Polymer International,* 2013, **20**, 1-15.

14. S. L. Ruan, P. Gao and T. X. Yu, *Polymer*, 2006, **47**, 1604-1611.

15. J. T. Yeh, S. C. Lin, K. N. Chen and K. S. Huang, *Journal of Applied Polymer Science,* 2008, **110**, 2538-2548.

16. J. T. Yeh, Z. W. Wu, Y. C. Lai, Q. C. Li and P. Hu, *Polymer Engineering and Science*, 2011, **51**, 2552-2563.

17. J. T. Yeh, Z. W. Wu, Y. C. Lai, H. P. Zhou and Q. Zhou, *Polymer Engineering and Science* , 2011, **51**, 687-696.

18. Yeh JT, Lai YC, Liu H, Shu YC and Huang CY, *Polymer International,* 2011, **60**, 59-68.

19. J. T. Yeh, C. C. Tsai, C. K. Wang, M. Z. Xiao and S. C. Chen, *Carbohydrate Polymers,* 2014, **101**, 1-10.

20. S. Iijima, *Nature,* 1991, **354**, 56-58.

21. J. Wang, Z. B. Wang, J. Li, P. Chen, M. H. Miao and Q. Gu, *Carbohydrate Polymers,* 2012, **87**, 784-789.

22. B. J. Wang, J. Li, J.Q. Zhang, H. Y. Li, P. Chen, Q. Gu and Z. B. Wang, *Carbohydrate Polymers,* 2013, **95**, 100-106.

23. Heath L, Zhu L and Thielemans W, *Chem Sus Chem,* 2013, **6**, 537-544.

24. A. Dufresne, *Canadian Journal of Chemistry-Revue Canadienne De Chimie,* 2008, **86**, 484-494.

25. N. Lin, J. Huang and A. Dufresne, *Nanoscale,* 2012, **4**, 3274-3294.

26. A. Dufresne, M. B. Kellerhals and B. Witholt, *Macromolecules,* 1999, **32**, 7396-7401.

27. F. Zhang, F. Mei and X. Z. Wang, *Chin Chem Lett,* 2006, **17**, 833-836.

28. J. M. Williams, A. Adewunmi and R. M. Schek, *Biomaterials,* 2005, **26**, 48174827.

29. A. S. Goldstein, T. M. Juarez, C. D. Helmke, M. C. Gustin and A. G. Mikos, *Biomaterials,* 2001, **22**, 1279-1288.

30. M. G. Liu, J. D. Huang, B. H. Luo and C. G. Zhou, *International Journal of Biological Macromolecules,* 2015, **78**, 23-31.

31. J. unkasem, R. Rujiravanit and P. Supaphol, *Nanotechnology*, 2006, **17**, 4519-4528.

32. M. Paillet and A. Dufresne, *Macromolecules,* 2001, **34**, 6527-6530.

33. F. Tian, L. X. Hong and Y. Z. Wang, *Nucl Sci Tech,* 2015, **26**, 1-6.

34. A. P. Hammersley, S. O. Svensson and A. Thompson, *Nuclear Instrument and Methods in Physics Research Section A,* 1994, **346,** 312-321.

35. A. J. Pennings and A. Zwijnenburg, *J Polym Sci Polym Phys Ed*, 1979, **17**, 1011-1032.

36. N. Wang, E. Y. Ding, S. Chen, *Acta Polymerica Sinica*, 2006, **8**, 925-928.

37. L. E. Alexander, *X-ray Diffraction in Polymer Science Wiley: New York*, 1969.

38. W. Ruland, *J Polym Sci A Polym Symp,* 1969, **28**, 143-151.

39. W. Ruland and R. Perret, *J Appl Crystallogr,* 1969, **2**, 209-218.

40. W. Ruland and R. Perret, *J Appl Crystallogr*, 1970, **3**, 525-532.

Table 1

Samples identification and CNC and ACNC content in the UHMWPE composite fibers.

Table 2

The tensile properties of pure UHMWPE fibers, UHMWPE/CNC fibers and UHMWPE/ACNC fibers.

Table 3

The melting temperature (T_m), the decomposition temperature at 5 % weight loss ($T_{d,\,5\,\%}$) and at the maximum rate ($T_{d,\ max}$) of pure UHMWPE fibers, UHMWPE/CNC fibers and UHMWPE/ACNC fibers.

Table 4

The crystallinity and crystalline orientation fraction of pure UHMWPE fibers, UHMWPE/CNC fibers and UHMWPE/ACNC fibers: (1) f_{110}, due to the orientation fraction of 110 planes, (2) f_{200}, due to the orientation fraction of 200 planes.

Table 5

The average shish length ($\langle L_{shish} \rangle$) and the shish misorientation ($B_{\emptyset}$) of pure UHMWPE fibers, UHMWPE/CNC fibers and UHMWPE/ACNC fibers.

Fig.1. The stress–strain curves for pure UHMWPE fibers, UHMWPE/CNC fibers, and UHMWPE/ACNC fibers stretched at the rate of 250 mm/min and at the ambient temperature.

Fig.2. DSC thermograms of pure UHMWPE fibers, UHMWPE composite fibers with various content of CNC or ACNC: (a) pure UHMWPE fibers, (b) 0.5 % CNC, (c) 0.5 % ACNC, (d) 1.0 % CNC, (e) 1.0 % ACNC.

Fig.3. TGA curves of pure UHMWPE fibers, UHMWPE/CNC fibers and UHMWPE/ACNC fibers in a N_2 atmosphere at a heating rate of 10 °C/min.

Fig.4. The 2D WAXD and SAXS images of pure UHMWPE fibers, UHMWPE/CNC fibers and UHMWPE/ACNC fibers: (a) pure UHMWPE fibers, (b) UHMWPE/CNC0.5 fibers, (c) UHMWPE/ACNC0.5 fibers, (d) UHMWPE/CNC1.0 fibers, (e) UHMWPE/ACNC1.0 fibers.

Fig.5. SEM images of different stage of pure UHMWPE fibers: (a, b) the drawn fibers at first hot-drawing stage, (c, d) the produced fibers.

Fig.6. 1D WAXD intensity profiles of pure UHMWPE fibers, UHMWPE/CNC fibers and UHMWPE/ACNC fibers: (a) pure UHMWPE fibers, (b) UHMWPE/CNC0.5 fibers, (c) UHMWPE/ACNC0.5 fibers, (d) UHMWPE/CNC1.0 fibers, (e) UHMWPE/ACNC1.0 fibers.

Fig.7. Plot of azimuthal integral width (B_{obs}) vs the value of $1/s$, which was used to determine the average shish length ($\langle L_{shish} \rangle$) and the shish misorientation ($B_{\emptyset}$) based on eq 4.

Table 1

Samples identification and CNC and ACNC content in the UHMWPE composite fibers.

Sample	CNC (wt%)	ACNC (wt%)
Pure UHMWPE fibers	0	0
UHMWPE/CNC0.5 fibers	0.5	-
UHMWPE/ACNC0.5 fibers	-	0.5
UHMWPE/CNC1.0 fibers	1.0	-
UHMWPE/ACNC1.0 fibers	-	1.0

Table 2

The tensile properties of pure UHMWPE fibers, UHMWPE/CNC fibers and UHMWPE/ACNC fibers.

Sample	Tensile strength (GPa)	Young's modulus (GPa)	Ultimate Elongation (%)
Pure UHMWPE fibers	2.60±0.12	125.7±6.9	3.11±0.15
UHMWPE/CNC0.5 fibers	2.79±0.17	141.6±6.5	2.77±0.13
UHMWPE/ACNC0.5 fibers	2.84±0.18	142.7±8.0	2.67±0.06
UHMWPE/CNC1.0 fibers	2.98±0.17	147.1±6.7	2.63±0.19
UHMWPE/ACNC1.0 fibers	3.07±0.17	152.5±6.0	2.59±0.08

Table 3

The melting temperature (T_m), the decomposition temperature at 5 % weight loss ($T_{d,\,5\,\%}$) and at the maximum rate ($T_{d,\,max}$) of pure UHMWPE fibers, UHMWPE/CNC fibers and UHMWPE/ACNC fibers.

Sample	T_m (◦C)	$T_{d,\,5\%}$ (◦C)	$T_{d,\,max}$ (◦C)
Neat UHMWPE fibers	147.17	300	471
UHMWPE/CNC0.5 fibers	147.43	302	473
UHMWPE/ACNC0.5 fibers	147.71	308	472
UHMWPE/CNC1.0 fibers	147.74	313	475
UHMWPE/ACNC1.0 fibers	147.64	316	472

Table 4

The crystallinity and crystalline orientation fraction of pure UHMWPE fibers, UHMWPE/CNC fibers and UHMWPE/ACNC fibers: (1) f_{110}, due to the orientation fraction of 110 planes, (2) f_{200}, due to the orientation fraction of 200 planes.

Sample	Crystallinity (%)	f_{110}	f_{200}
Pure UHMWPE fibers	72.3	0.947	0.935
UHMWPE/CNC0.5 fibers	73.3	0.912	0.889
UHMWPE/ACNC0.5 fibers	74.2	0.914	0.894
UHMWPE/CNC1.0 fibers	77.5	0.910	0.893
UHMWPE/ACNC1.0 fibers	84.5	0.914	0.883

Table 5

The average shish length ($\langle L_{shish} \rangle$) and the shish misorientation ($B_{\emptyset}$) of pure UHMWPE fibers, UHMWPE/CNC fibers and UHMWPE/ACNC fibers.

Sample	$\langle L_{shish} \rangle$ (nm)	$B_{\emptyset}$ (degree)
Pure UHMWPE fibers	770	4.69
UHMWPE/CNC0.5 fibers	748	4.36
UHMWPE/ACNC0.5 fibers	845	6.28
UHMWPE/CNC1.0 fibers	717	3.91
UHMWPE/ACNC1.0 fibers	953	7.37

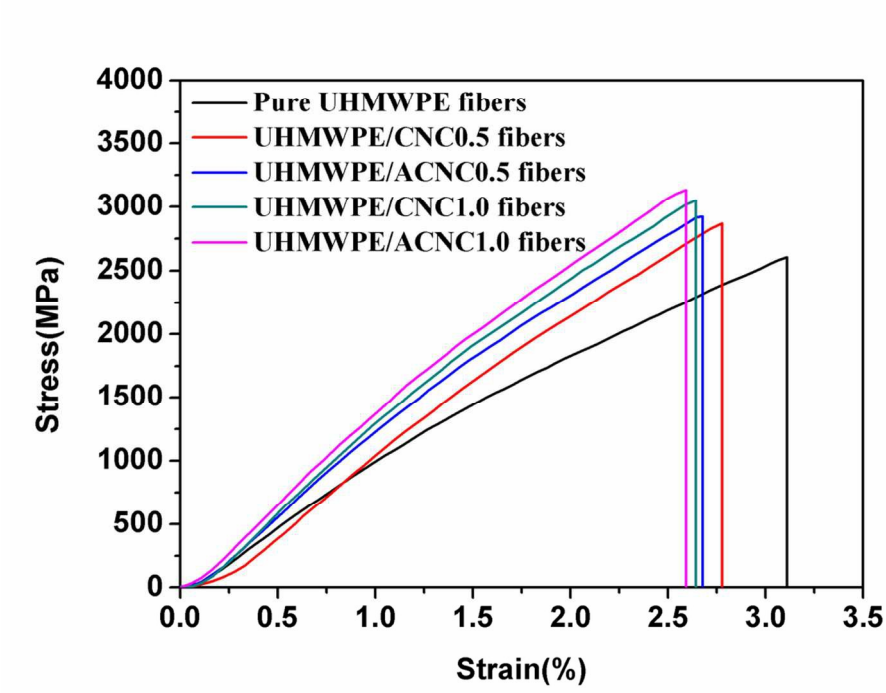

Fig.1. The stress–strain curves for pure UHMWPE fibers, UHMWPE/CNC fibers, and UHMWPE/ACNC fibers stretched at the rate of 250 mm/min and at the ambient temperature.
52x37mm (600 x 600 DPI)

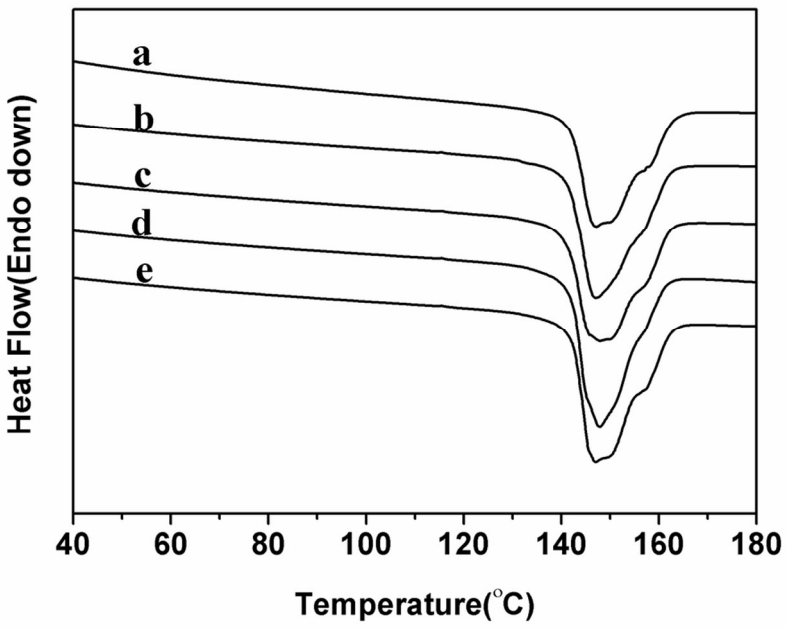

Fig.2. DSC thermograms of pure UHMWPE fibers, UHMWPE composite fibers with various content of CNC or ACNC: (a) pure UHMWPE fibers, (b) 0.5 % CNC, (c) 0.5 % ACNC, (d) 1.0 % CNC, (e) 1.0 % ACNC.
52x36mm (600 x 600 DPI)

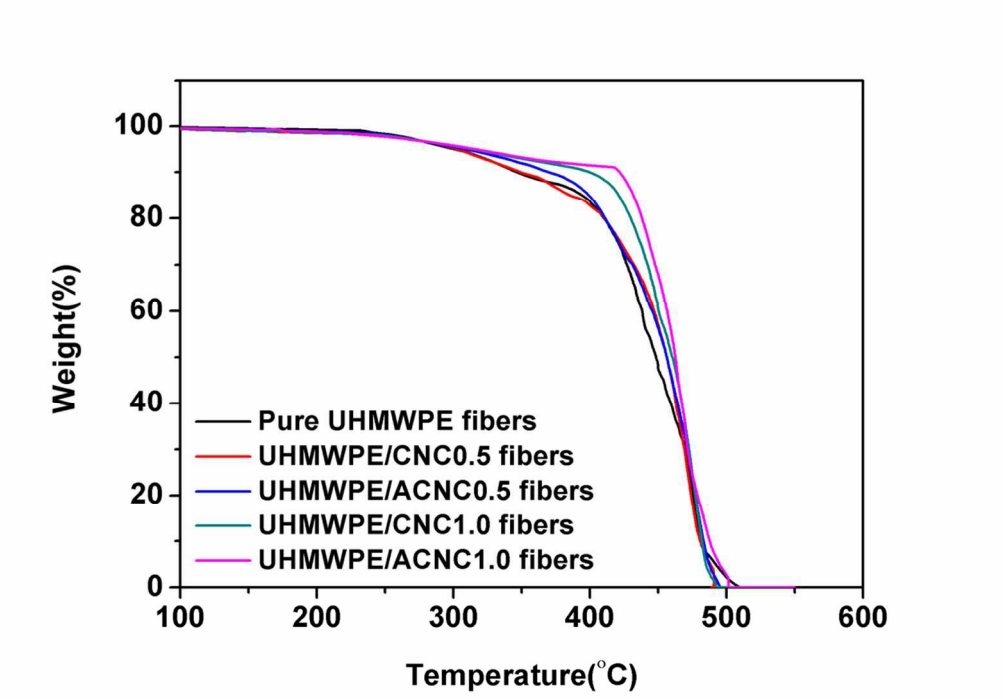

Fig.3. TGA curves of pure UHMWPE fibers, UHMWPE/CNC fibers and UHMWPE/ACNC fibers in a N2 atmosphere at a heating rate of 10 °C/min.
52x37mm (600 x 600 DPI)

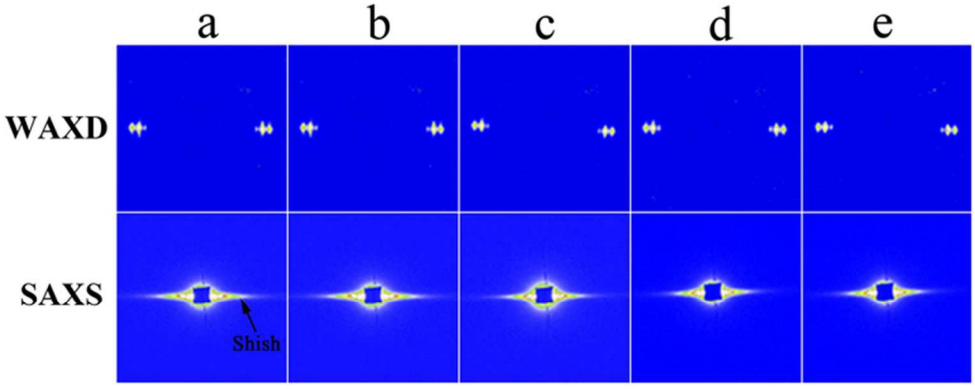

Fig.4. The 2D WAXD and SAXS images of pure UHMWPE fibers, UHMWPE/CNC fibers and UHMWPE/ACNC fibers: (a) pure UHMWPE fibers, (b) UHMWPE/CNC0.5 fibers, (c) UHMWPE/ACNC0.5 fibers, (d) UHMWPE/CNC1.0 fibers, (e) UHMWPE/ACNC1.0 fibers.
33x13mm (600 x 600 DPI)

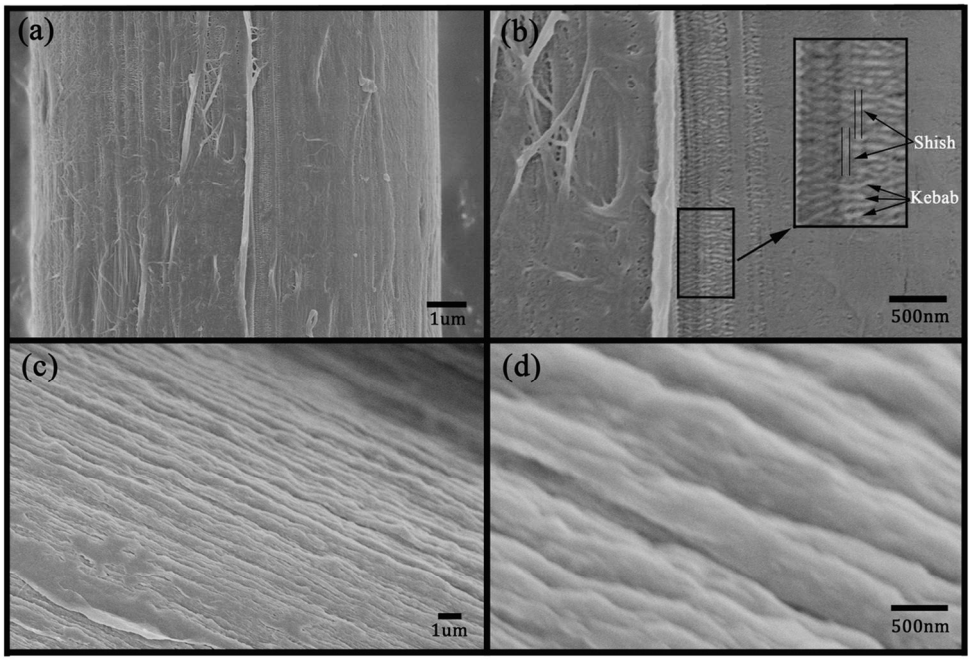

Fig.5. SEM images of different stage of pure UHMWPE fibers: (a, b) the drawn fibers at first hot-drawing stage, (c, d) the produced fibers.
56x38mm (600 x 600 DPI)

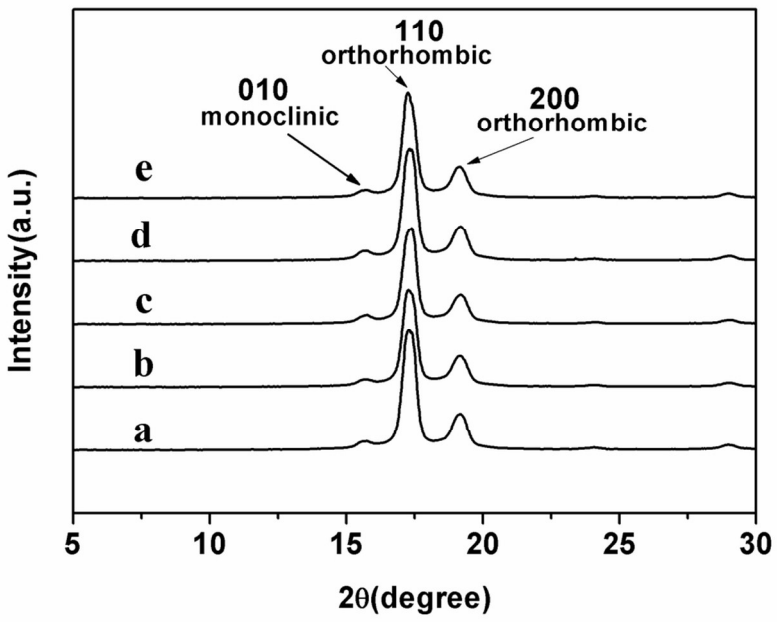

Fig.6. 1D WAXD intensity profiles of pure UHMWPE fibers, UHMWPE/CNC fibers and UHMWPE/ACNC fibers: (a) pure UHMWPE fibers, (b) UHMWPE/CNC0.5 fibers, (c) UHMWPE/ACNC0.5 fibers, (d) UHMWPE/CNC1.0 fibers, (e) UHMWPE/ACNC1.0 fibers.
52x36mm (600 x 600 DPI)

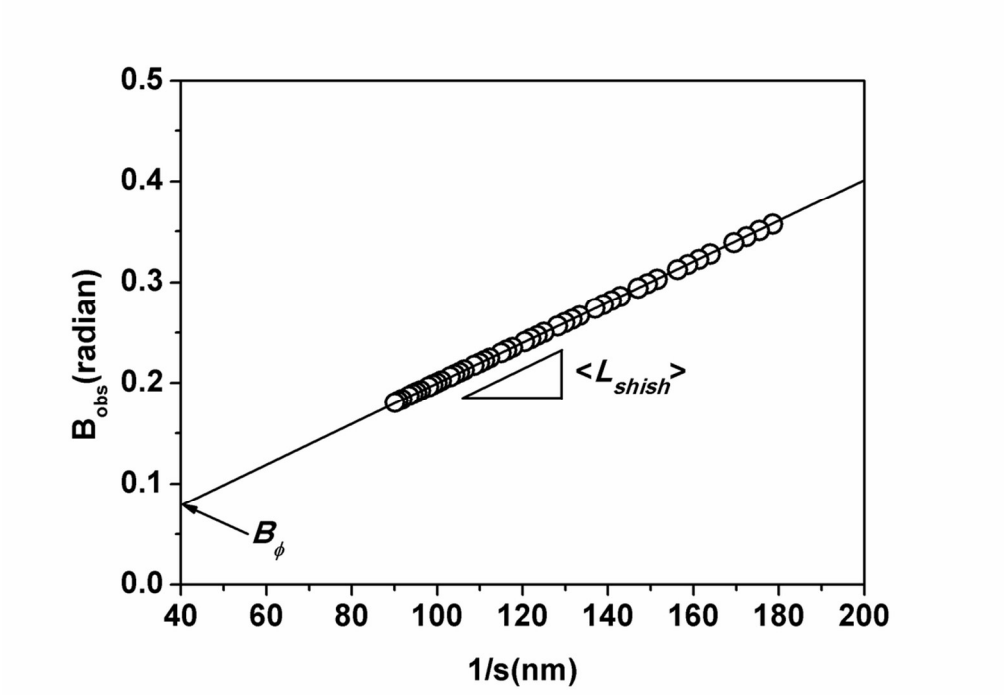

Fig.7. Plot of azimuthal integral width (B_obs) vs the value of 1/s, which was used to determine the average shish length (⟨L_shish ⟩) and the shish misorientation (〖 B〗 _∅) based on eq 4.
52x36mm (600 x 600 DPI)